The Novel SLIM Method for the Determination of the Iron Core Saturation Level in Induction Motors

Gyftakis, K

Original citation & hyperlink:
Gyftakis, K 2017, The Novel SLIM Method for the Determination of the Iron Core Saturation Level in Induction Motors. in *2016 IEEE Energy Conversion Congress and Exposition (ECCE).* IEEE, IEEE Energy Conversion Congress and Expo 2016, Milwaukee, United States, 18-22 September
https://dx.doi.org/10.1109/ECCE.2016.7855506

DOI 10.1109/ECCE.2016.7855506
ISBN 978-1-5090-0738-7
ESBN 978-1-5090-0737-0

Publisher: IEEE

The Novel SLIM Method for the Determination of the Iron Core Saturation Level in Induction Motors

Konstantinos N. Gyftakis
School of CEM and Research Centre for Mobility and Transport
Coventry University
Coventry, UK
k.n.gyftakis@ieee.org

***Abstract*— Lately, a new diagnostic mean has been introduced for reliable fault diagnosis in delta-connected induction motors. This diagnostic mean is the zero-sequence current frequency spectrum. It will be shown in this paper that, the zero-sequence current waveform can be reliably used for identifying the induction motor's iron core saturation level. So in this work, simulations with the Finite Element Method and experimental testing are carried out, with the healthy induction motor operating under different load levels. The paper proposes a novel method called SLIM for reliable induction motor saturation level determination.**

Keywords— FEM; harmonic index; induction motor; saturation; zero-sequence current

NOMENCLATURE

v	Integer
θ, φ	Phase angles
ω_s	Stator angular frequency
A, B, Γ	Amplitudes
f_s	Stator frequency
$fund$	Indicator for fundamental
i_{zsc}	Zero-sequence current
k, l	Integers
p	Number of pole pairs
s	Slip
s_2	Rotor slot number
sat	Indicator for saturation
st_MMF	Indicator for stator Magnetomotive force.
t	Time
RSH	Indicator for rotor slot harmonics

I. INTRODUCTION

THE induction motor iron core saturation has a strong impact on its operation and electromagnetic characteristics. As a phenomenon, it is related to the induction motor operating electromagnetic characteristics [1]-[2] and efficiency [3]-[7], spatial and time-dependant electromagnetic variables' harmonic index [8]-[15], fault diagnosis issues [16]-[21], parameter estimation [22] etc. The knowledge of operating parameters is crucial because it affects the machine and drive performance [23]-[24]. Moreover, the optimization of the induction motor design is strongly affected by the laminations saturation level and operating point [25]. Finally, the saturation together with other phenomena, like the slotting and the motion, produce increased higher harmonic index in the magnetic field [26], which result in increased torque ripple, vibrations and noise [27], which mean more frequent need for maintenance.

Throughout the literature, the determination of the induction motor saturation level is possible through the monitoring of the stator line current third harmonic's amplitude [17]-[18]. The information provided through this specific harmonic has been used as an extra observation regarding how the saturation affects the healthy and faulty operating conditions of the induction motor. The knowledge of every motor parameter regarding its functioning conditions in real time is crucial for reliable and safe operation.

Unfortunately, this specific iron core saturation level determination has many and serious drawbacks. To begin with, the third stator line current harmonic is affected by the voltage supply imbalance [18], [28]. Moreover, it is also affected by the stator inter-turn faults [29]-[32]. Furthermore, this specific harmonic is influenced by inherent machine asymmetries such as the asymmetrical wiring [32]. Finally, the third line current harmonic's amplitude differs from motor to motor and as a consequence, the determination of the saturation level requires a full knowledge and measurements of each different motor separately. So, it is not possible through the third current harmonic amplitude monitoring to determine the saturation level of a motor which has not be measured in the past and is met for the first time. All by all, it occurs that, the existence of a generalized saturation monitoring method, independent from the motor's geometrical and electromagnetic characteristics could be a valuable tool in the area of condition monitoring.

The answer to this need is the zero-sequence current. The zero-sequence current frequency spectrum has proved to be a valuable diagnostic mean lately [33]-[35]. It reliably deals with a variety of delta-connected induction motor faults such as the static eccentricity (even when the motor produces Principle Slot Harmonics-PSH), the broken bar fault, the

supply imbalance and the stator inter-turn fault.

The paper's original contribution is the development of a novel technique for accurate saturation level identification in induction motors. The technique is not affected by the induction motor geometrical characteristics and thus can be applied in any induction motor case. The method has been named SLIM (Saturation Level of Induction Motor) method. The method's effectiveness by using FEM simulations and experimental testing, has been studied using a 3-phase, 4-pole, 4kW, 400V, 50Hz, PSH-induction motor with 36 stator and 28 rotor slots. Finally, the method is applied to a 6.6kV, 1.1MW industrial induction motor using FEM.

II. Analytical Calculations

In the lately published paper [33], the harmonic index of the zero-sequence current spectrum in a delta-connected induction motor was thoroughly presented and explained, with the use of analytical formulas.

Briefly, it was shown that the zero-sequence current spectrum of a symmetrical delta-connected induction motor, which is fed by a symmetrical 3-phase sinusoidal voltage system, will be:

$$i_{zsc}(t) = i_{zsc}(t)_{st\_MMF} + i_{zsc}(t)_{sat} + i_{zsc}(t)_{RSH} \quad (1)$$

Where:

$$i_{zsc}(t)_{st\_MMF} = 3\sum_{v=3k,k=odd}^{\infty} I_v \cos(v\omega_s t) \quad (2)$$

$$i_{zsc}(t)_{sat} = 3\sum_{v=3k,k=odd}^{\infty} I_{v\_sat} \cos(v\omega_s t + \varphi_{sat}) \quad (3)$$

$$i_{zsc}(t)_{RSH} = \sum_{v=6k\pm1}^{\infty} I_{v\_RSH} \cos[(ls_2\omega_2 \pm v\omega_s)t + \varphi_{RSH}] \quad (4)$$

The first term (eq. 2) is due to the phase current MMF harmonics. The second term (eq. 3) is related to the level of the iron core saturation. Finally, the last term (eq. 4) is related to the number of the rotor slots. This term is zero if the rotor slot number is multiple of three. The motor used in this paper has 28 rotor slots, which is not a multiple of three. As a consequence, in this induction motor case the zero-sequence current will additionally contain higher harmonic index, located at frequencies $\left[l(1-s)s_2/p \pm v\right]f_s$.

The above concern symmetrical induction motors. This means that the induction motor does not have manufacturing inherent asymmetries. Moreover, the 3-phase supply voltage is also ideally symmetrical.

Furthermore, it is interesting that, equations (2) and (3) contain harmonics located at the same frequencies, but with a phase difference. So, for the fundamental zero-sequence current harmonic there stands:

$$i_{zsc}(t)_{fund} = A\cos(3\omega_s t) + B\cos(3\omega_s t + \varphi_{sat}) \quad (5)$$

Equation (5), with the use of trigonometry, can be also expressed as:

$$i_{zsc}(t)_{fund} = \Gamma\cos(3\omega_s t + \theta) \quad (6)$$

Where:

$$\Gamma = \sqrt{A^2 + B^2 + 2AB\cos(\varphi_{sat})}$$

and

$$\theta = \arctan\left[\frac{B\sin(\varphi_{sat})}{A + B\cos(\varphi_{sat})}\right]$$

The equation (6) clearly shows that the amplitude of the fundamental zero-sequence current harmonic depends on both amplitudes of the stator MMF 3rd phase current harmonic and saturation harmonic as well. Additionally, the level of the saturation influences the phase angle θ.

III. FEM Results

Firstly, an induction motor FEM model has been created and simulated to operate under nominal load 30Nm, as well as under low load operation 3Nm. The model takes its characteristics accordingly to the real motor, which has been tested in the Laboratory. All its geometrical and materials characteristics are well known from the manufacturer's blueprints. Due to high simulation time, the FEM motor model has been considered un-skewed.

Fig. 1 and Fig. 2 illustrate the phase and zero-sequence currents versus time for 30Nm and 3Nm respectively. The speed occurred about 1465rpm and 1494rpm for the two above cases respectively.

It can be seen that, the phase and zero-sequence currents contain an important portion of higher harmonics. That is because the studied motor due to its rotor slot and magnetic poles numbers produces increased rotor slot harmonics. Those harmonics are not filtered because the motor has been simulated without skew.

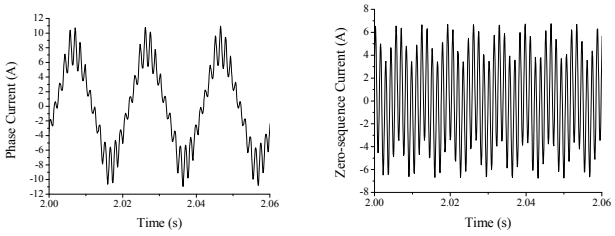

a) b)

Fig. 1. FEM results of the: a) phase and b) zero-sequence currents for motor operation under 30Nm applied load.

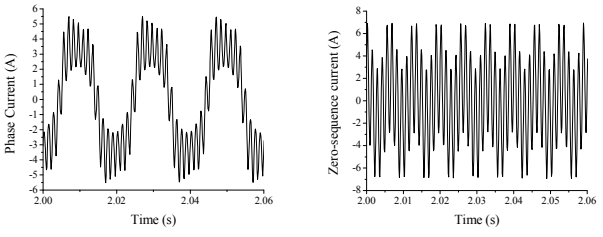

a) b)

Fig. 2. FEM results of the: a) phase and b) zero-sequence currents for motor operation under 3Nm applied load.

Moreover, the spatial distribution of the magnetic flux density amplitude for 30Nm and 3Nm applied mechanical load are presented in Fig. 3. As expected, the low load operation is escorted by increased induction motor saturation level.

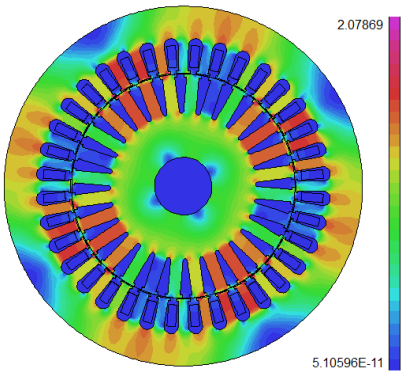

a)

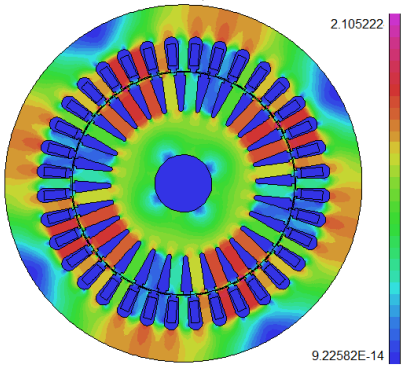

b)

Fig. 3. The spatial distribution of the magnetic flux density amplitude for: a) 30Nm and b) 3Nm applied load.

IV. EXPERIMENTAL TESTING

The delta connected induction motor has been coupled to a DC generator, feeding a variable ohmic resistance. The motor is fed by the grid with 3-phase, sinusoidal, 380V voltage supply. Eight different load/speed levels have been set and measured. For all cases, the phase current and zero-sequence current waveforms (Fig. 4) are illustrated. The rated phase current values are shown for each case in Table I.

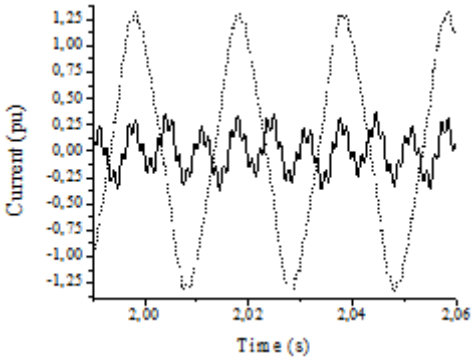

a)

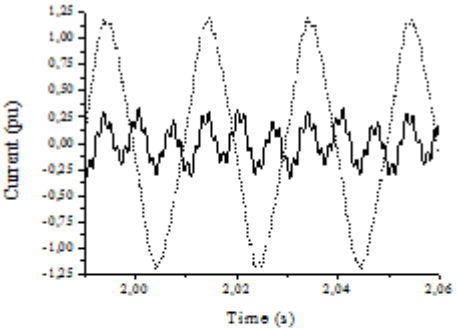

b)

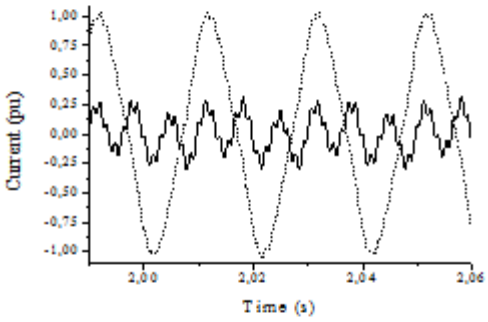

c)

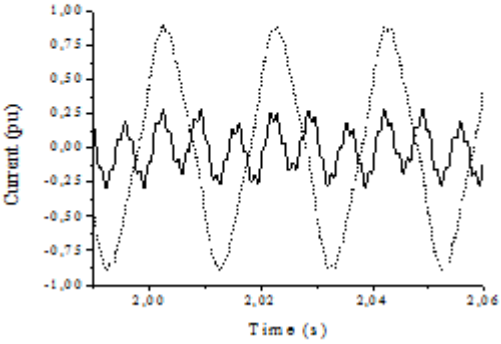

d)

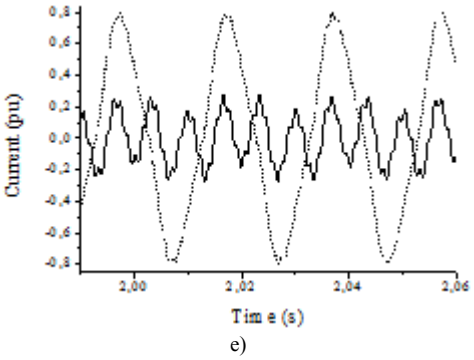

e)

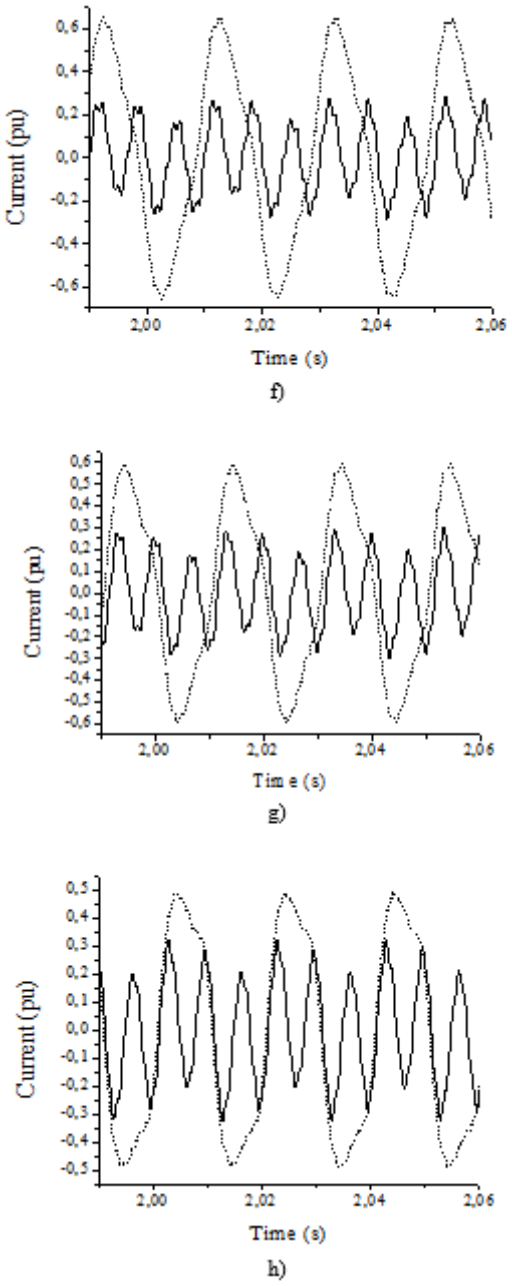

Fig. 4. The phase (dash) and zero-sequence (solid) current waveforms versus time for speed: a) 1427, b) 1438, c) 1450, d) 1460, e) 1467, f) 1478 g) 1485 and h) 1494rpm.

TABLE I
RATED PHASE CURRENT VERSUS SPEED

Speed (rpm)	1427	1438	1450	1460	1467	1478	1485	1494
Current (A)	9.4	8.4	7.2	6	5.3	4.3	3.8	2.8

V. DISCUSSION

In this paragraph, the FEM and experimental results will be thoroughly discussed.

Firstly, the impact of the saturation level is clearly expressed through the zero-sequence current waveform, obeying to the calculated equation (6). The FEM simulations show that, the zero-sequence current amplitude remains practically the same while the motor operates with two different load cases (Fig. 1-Fig. 2). At the same time, the phase current amplitude decreases while the load decreases too, as expected. Moreover, while difficult because of the high harmonic index of the zero-sequence current waveforms, a closer look reveals that the phase difference between the phase and zero-sequence currents has been changed. More specifically it seems that in Fig. 1, the third zero-sequence current harmonic and the phase fundamental harmonic have a phase difference about 180degrees, while in Fig. 2 the phase current has been shifted by an angle close to 180 degrees, relatively to the zero-sequence current waveform and thus their phase difference is close to zero.

The experimental results support the simulation ones with success. In the first six load cases (Fig. 4a-f), the zero-sequence current remains practically the same in amplitude, while the phase current decreases with the increment of the speed. Then in the last two cases (Fig. 4g-h), when the speed is close to the synchronous one, a slight increase in the zero-sequence current amplitude can be observed.

Moreover, the phase difference between the phase and the zero-sequence current waveforms seems to be close to 0 degrees, for induction motor speed 1427rpm-1460rpm (Fig. 1a-d). On the other hand, in the other speed cases, a gradual shifting of the zero-sequence current waveform, to the left of the phase current waveform, is observed. Finally, in the last case (Fig. 1h) the phase angle between the two waveforms comes close to 180 degrees. The last case is a low-load condition, where the saturation level is greatly increased.

The FEM and experimental results clearly obey to Paragraph II, equation (5). It was shown that the zero-sequence current fundamental harmonic consists of two terms: the stator MMF term and the saturation related one. Consequently, while the load decreases the phase current decreases too. So, the stator MMF related third harmonic component decreases. At the same time, the decrease of the load causes higher saturation level (Fig. 3). The second term of equation (5) is related to the saturation and thus it increases in amplitude, while the load decreases. The above situation results to a high zero-sequence amplitude even at no-load operation.

At the same time, the two terms of equation (5) have a phase difference. So, their sum clearly affects the phase of the zero-sequence current waveform (equation (6)).

It is clear that, the relation between the phase and zero-sequence current waveforms proves to be a valuable tool for the estimation of the induction motor saturation level. As a consequence a better technique has to be applied in order to get the saturation level information reliably. This is why the Lissajous diagrams technique is adopted.

VI. THE SLIM METHOD RESULTS

Lissajous diagrams are very informative when it comes to compare the amplitude and phase differences between two signals. That is why they are selected to be used in this specific investigation. The phase current versus the zero-sequence current diagrams are presented in Fig. 5 for the FEM simulation results. Moreover, the experimental Lissajous diagrams are illustrated in Fig. 6.

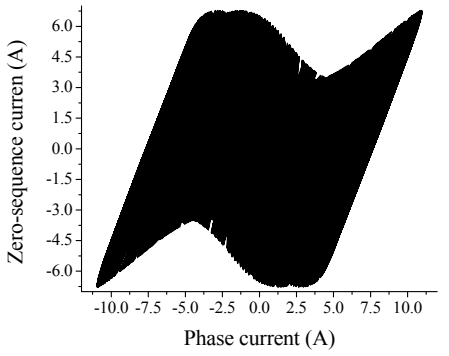

a)

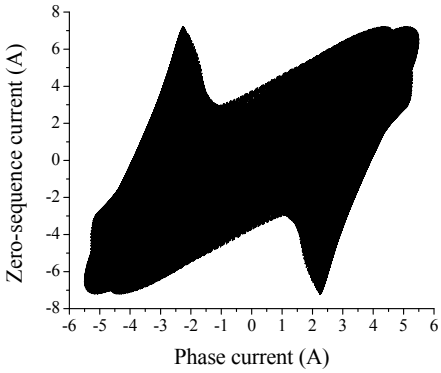

b)

Fig. 5. Lissajous diagram of the zero-sequence current versus the phase current for: a) 30Nm and b) 3Nm applied mechanical load (FEM simulation results).

It can be seen in Fig. 5 that the rotor slot related harmonics play indeed an important role to the Lissajous configuration. On the other hand, the presence of the skewing decreases their amplitudes and so the experimental results (Fig. 6) clearly reveal the fundamental zero-sequence current harmonic. Despite that, the aspect ratio of the resulting ellipse, which is a function of the phase shift between the two signals is the same while comparing the FEM and the experimental results.

The saturation level information is clearly shown with the SLIM method. It is shown in Fig. 6-a,b that the motor has low saturation level and it is operating at the linear part of the iron core B-H magnetic characteristic. When the speed increases even more, then the gradient phase shifting between the phase and zero-sequence currents is observed. At the same time, it is easy to observe the amplitude difference between them. In Fig. 6-f,g three distinct ellipsis are clearly observed. So, somewhere close to 1478rpm, the stator MMF and the saturation-related third harmonic components become the same in amplitude within the zero-sequence current. That is because the ellipsis acquires an aspect ratio close to 1 (circle). Finally, the saturation is clearly dominant inside the motor, for speed 1494, since the ellipsis surface has been significantly decreased (phase difference close to 180 degrees).

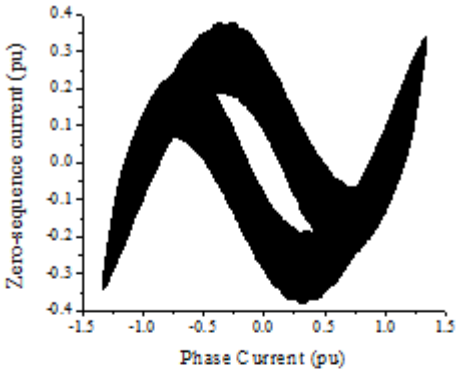

a)

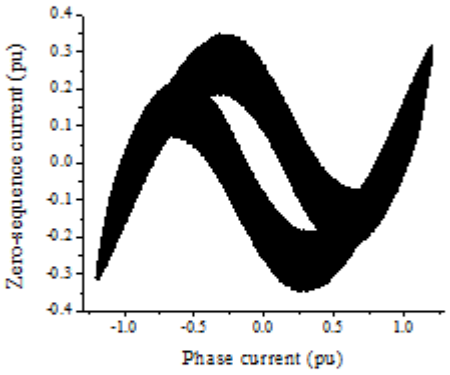

b)

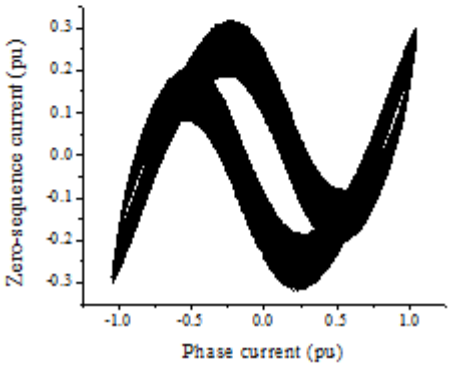

c)

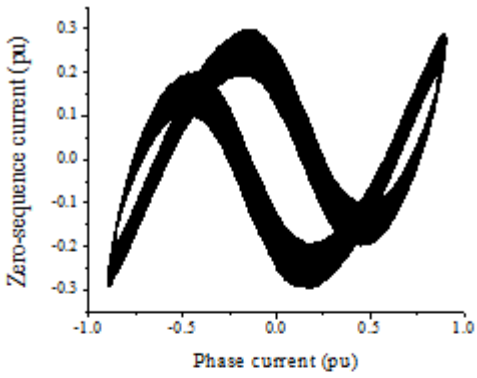

d)

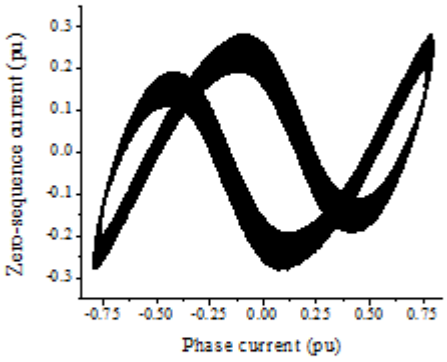

e)

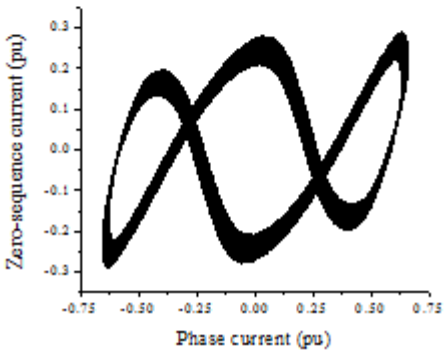

f)

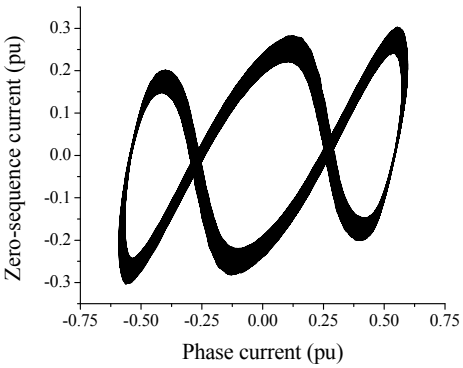

g)

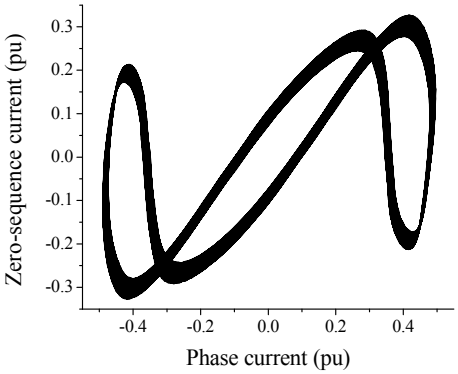

h)

Fig. 6. Lissajous diagrams of the zero-sequence current versus the phase current for speed: a) 1427, b) 1438, c) 1450, d) 1460, e) 1467, f) 1478 g) 1485 and h) 1494rpm (experimental results).

VII. Application of the SLIM Method on a Large Industrial Motor

In this section, the SLIM method is applied a newly manufactured industrial 6.6kV, 1.1MW, 6-pole, three-phase cage induction motor, whose geometrical and material data are known by the manufacturer blueprints. So, an accurate FEM model was created and simulated to operate at nominal load 1.1MNm. The spatial distribution of the motor's magnetic flux density amplitude is shown in Fig. 7. Furthermore, the SLIM method's result is illustrated in Fig. 8. The rotor slot harmonics greatly influence the zero-sequence current. So, a low-pass filter was applied to cut frequencies above 200Hz. The third harmonic, which was included in the zero-sequence current compared to the original zero-sequence current's waveform is shown in Fig. 9. After the filtering, the Lissajous diagram of the third zero-sequence harmonic versus the phase current is illustrated in Fig. 10. Finally, the motor was simulated to operate under double nominal load 2.2MNm and the SLIM method's result is shown in Fig. 11. This study's conclusion is that the newly manufactured induction motor has been well designed, as far as the saturation effect is considered, thus it cannot be easily saturated, probably because of the much larger rotor and stator yoke compared to smaller induction motors. It has to be noted that, the operation speed of this motor is very close to the synchronous speed. More specifically, the speed is 996.6rpm and 990.6rpm for operation under nominal load 1.1MNm and under 2.2MNm respectively.

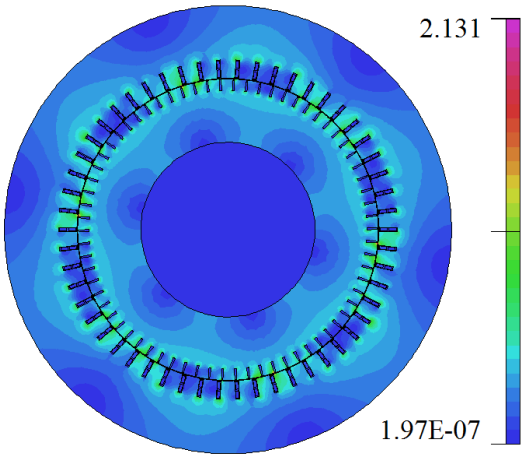

Fig. 7. Spatial distribution of the magnetic flux density amplitude of the 1.1MW induction motor (1.1MNm).

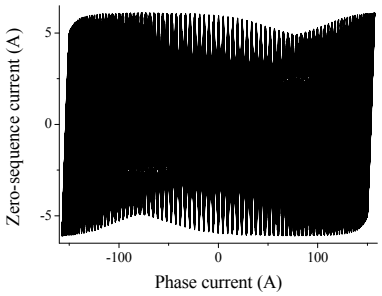

Fig. 8. Lissajous diagrams of the zero-sequence current versus the phase current for the 1.1MW induction motor (FEM simulation results-1.1MNm).

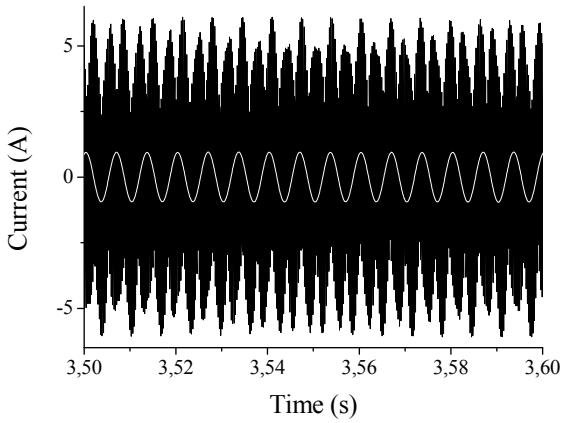

Fig. 9. The zero-sequence current before (black) and after (white) filtering (Nominal load 1.1MNm).

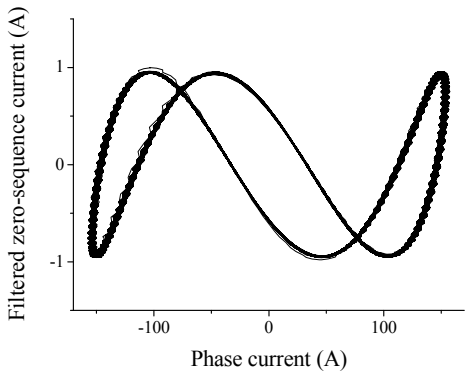

Fig. 10. The filtered zero-sequence current versus the phase current for the 1.1MW induction motor (FEM simulation results-1.1MNm).

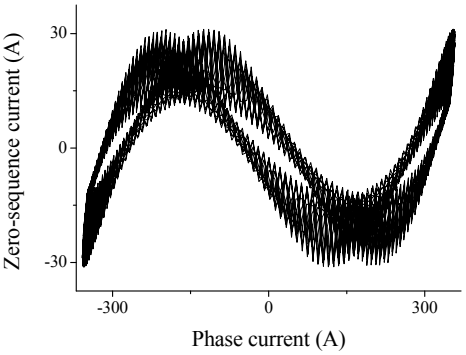

Fig. 11. Lissajous diagrams of the zero-sequence current versus the phase current for the 1.1MW induction motor (FEM simulation results-2.2MNm).

VIII. CONCLUSION

In this paper, the novel SLIM method is illustrated. It is shown with the use of analytical calculations, FEM simulations and experimental testing that, the Lissajous diagrams of the zero-sequence and phase currents provide a reliable tool for determining the induction motor saturation level. The proposed method's distinct advantage compared to the traditional observation of the line current's third harmonic amplitude is obvious because it is not affected by the motor's geometrical characteristics, like the rotor slot number. It is a method which can be very helpful during the design/manufacturing stage of the induction motor. Also, it could be used as supplementary information, while performing condition monitoring in induction motors. A limitation of the proposed method in its present form is that, in order to be applied in star-connected induction motors it is necessary to have the neutral connected.

REFERENCES

[1] W. Liang, J. Wang, T. Iu and W. Fang, "A New Method for Multiple Finite-Element Models in Cosimulation With Electrical Circuit Using Machine Multiloop Modeling Scheme," *IEEE Trans. Ind. Elec.*, Vol. 61, No. 12, pp. 6583-6590, Dec. 2014.

[2] K. Wang, W. Yao, B. Chen, G. Shen, K. Lee and Z. Lu, "Magnetizing-Curve Identification for Induction Motors at Standstill without Assumption of Analytical Curve Functions," *IEEE Trans. Ind. Elec.*, early access paper, DOI: 10.1109/TIE.2014.2354012.

[3] M. Amrhein and P. T. Krein, "Induction Machine Modeling Approach Based on 3-D Magnetic Equivalent Circuit Framework", *IEEE Trans. Ener. Conv.*, Vol. 25, No. 2, pp. 339-347, Jun. 2010.

[4] Z. Gmyrek, A. Boglietti and A. Cavagnino, "Estimation of Iron Losses in Induction Motors: Calculation Method, Results and Analysis", *IEEE Trans. Ind. Elec.*, Vol. 57, No. 1, pp. 161-171, Jan. 2010.

[5] A. Boglietti, A. Cavagnino and M. Lazzari, "Computational Algorithms for Induction Motor Equivalent Circuit Parameter Determination-Part II: Skin Effect and Magnetizing Characteristics," *IEEE Trans. Ind. Elec.*, Vol. 58, No. 9, pp. 3734-3740, Sep. 2011.

[6] A. Belahcen and A. Arkkio, "Comprehensive Dynamic Loss Model of Electrical Steel Applied to FE Simulation of Electrical Machines", *IEEE Trans. Magn*., Vol. 44, No. 6, pp. 886-889, Jun. 2008.

[7] E. Dlala, A. Belahcen and A. Arkkio, "On the Importance of Incorporating Iron Losses in the Magnetic Field Solution of Electrical Machines", *IEEE Trans. Magn.*, Vol. 46, No. 8, pp. 3101-3104, Aug. 2010.

[8] D. J. Kim, J. W. Jung, J. P. Hong, K. J. Kim and C. J. Park, "A Study on the Design Process of Noise Reduction in Induction Motors", *IEEE Trans. Magn*., Vol. 48, No. 11, pp. 4638-4641, Nov. 2012.

[9] Z. Ling, L. Zhou, S. Guo and Y. Zhang, "Equivalent Circuit Parameters Calculation of Induction Motor by Finite Element Analysis*", IEEE Trans. Magn*., Vol. 50, No. 2, Article# 7020604, Feb. 2014.

[10] A. Tenhunen, T. P. Holopainen and A. Arkio, "Effects of Saturation on the Forces in Induction Motors With Whirling Cage Rotor", *IEEE Trans. Magn.*, Vol. 40, No. 2, pp. 766-769, Mar. 2004.

[11] G. Bottiglieri, A. Consoli and T. A. Lipo, "Modelling of Saturated Induction Machines With Injected High-Frequency Signals", *IEEE Trans. Ener. Conv*., Vol. 22, No. 4, pp. 819-828, Dec. 2007.

[12] M. Ikeda and T. Hiyama, "SImulation Studies of the Transients of Squirrel-Cage Induction Motors", *IEEE Trans. Ener. Conv*., Vol. 22, No. 2, pp. 233-239, Jun. 2007.

[13] O. Keysan and H. B. Ertan, "Real-Time Speed and Position Estimation Using Rotor Slot Harmonics", *IEEE Trans. Ind. Inf*., Vol. 9, No. 2, pp. 899-908, May 2013.

[14] S. Rainer, O. Biro, A. Stermecki and B. Weilharter, "Frequency Domain Evaluation of Transient Finite Element Simulations of Induction Machines", *IEEE Trans. Magn.,* Vol. 48, No. 2, pp. 851-854, Feb. 2012.

[15] G. M. Joksimovic, J. Riger, T. M. Wolbank, N. Peric and M. Vasak, "Stator-Current Spectrum Signature of Healthy Cage Rotor Induction Machines," *IEEE Trans. Ind. Elec*., Vol. 60, No. 9, pp. 4025-4033, Sep. 2013.

[16] J. Faiz, B. M. Ebrahimi and H. A. Toliyat, "Effect of Magnetic Saturation on Static and Mixed Eccentricity Fault Diagnosis in Induction Motor", *IEEE Trans. Magn*., Vol. 45, No. 8, pp. 3137-3144, Aug. 2009.

[17] M. Drif and A. J. M. Cardoso, "Stator Fault Diagnostics in Squirrel Cage Three-Phase Induction Motor Drives Using the Instantaneous Active and Reactive Power Signature Analyses", *IEEE Trans. Ind. Inf*., Vol. 10, No. 2, pp. 1348-1360, May 2014.

[18] S. Nandi, "A Detailed Model of Induction Machines With Saturation Extendable for Fault Analysis", *IEEE Trans. Ind. Appl*., Vol. 40, No. 5, pp. 1302-1309, Sep/Oct. 2004.

[19] J. Faiz, V. Ghorbanian and B. M. Ebrahimi, "EMD-Based Analysis of Industrial Induction Motors With Broken Rotor Bars for Identification of Operating Point at Different Supply Modes", *IEEE Trans. Ind. Inf*., Vol. 10, No. 2, pp. 957-966, May 2014.

[20] A. M. da Silva, R. J. Povinelli and N. A. O. Demerdash, "Rotor Bar Fault Monitoring Method Based on Analysis of Air-Gap Torques of Induction Motors", *IEEE Trans. Ind. Inf*., Vol. 9, No. 4, pp. 2274-2283, Nov. 2013.

[21] J. Sprooten and J.-C. Maun, "Influence of saturation level on the effect of broken bars in induction motors using fundamental electromagnetic laws and finite element simulations," *IEEE Trans. Ener. Conv.*, Vol. 24, No. 3, pp. 557–564, Sep. 2009.

[22] E. Laroche and M. Boutayeb, "Identification of the Induction Motor in Sinusoidal Mode", *IEEE Trans. Ener. Conv.,* Vol. 25, No. 1, pp. 11-19, Mar. 2010.

[23] T. Tuovinen, M. Hinkkanen and J. Luomi, "Modeling of Saturation Due to Main and Leakage Flux Interaction in Induction Machines*", IEEE Trans. Ind. Appl.*, Vol. 46, No. 3, pp. 937-945, May/Jun. 2010.

[24] K. Bradley, W. Cao, J. Clare and P. Wheeler, "Predicting inverter-induced harmonic loss by improved harmonic injection", *IEEE Trans. Power Elec.*, Vol. 23, No. 5, pp. 2619-2624, Sep. 2008.

[25] M. Centner and U. Schafer, "Optimized Design of High-Speed Induction Motors in Respect of the Electrical Steel Grade", *IEEE Trans. Ind. Elec*., Vol. 57, No. 1, pp. 288-295, Jan. 2010.

[26] E. Dlala, O. Bottauscio, M. Chiampi, M. Zucca, A. Belahcen and A. Arkkio, "Numerical Investigation of the Effects of Loading and Slot Harmonics on the Core Losses of Induction Machines", *IEEE Trans. Magn*., Vol. 48, No. 2, pp. 1063-1066, Feb. 2012.

[27] D. J. Kim, J. W. Jung, J. P. Hong, K. J. Kim and C. J. Park, "A Study on the Design Process of Noise Reduction in Induction Motors", *IEEE Trans. Magn*., Vol. 48, No. 11, pp. 4638-4641, Nov. 2012.

[28] K. N. Gyftakis, D. K. Athanasopoulos and J. C. Kappatou, "Broken Bar Fault Diagnosis in Single and Double Cage Induction Motors Fed by Asymmetrical Voltage Supply", IEEE 9th SDEMPED, Valencia, Spain, pp. 640-644, Sep. 2013.

[29] H. Henao, C. Demian and G.A. Capolino, "A frequency-domain detection of stator stator windings faults in induction machines using an external flux sensor," *IEEE Trans. Ind. Appl*., Vol. 39, No. 5, pp. 1272-1279, Sep./Oct. 2003.

[30] H. A. Toliyat, S. Nandi, S. Choi and H. Meshgin-Kelk, "Electric Machines-Modeling, Condition Monitoring and Fault Diagnosis," CRC Press, Taylor & Francis Group, pp. 117-118, 2013.

[31] G. Joksimovic and J. Penman, "The detection of interturn short circuits in the stator windings of operating motors," *IEEE Trans. Ind. Elec*., Vol. 47, No. 5, pp. 1078-1084, Oct. 2000.

[32] S. M. A. Cruz and A. J. M. Cardoso, "Diagnosis of stator inter-turn short circuits in DTC induction motor drives, "*IEEE Trans. Ind. Appl*., Vol. 40, No. 5, pp. 1349-1360, Sep/Oct. 2004.

[33] K. N. Gyftakis and J. C. Kappatou, "The Zero-Sequence Current as a Generalized Diagnostic Mean in Δ-Connected Three-Phase Induction Motors*," IEEE Trans. Ener. Conv*.,Vol. 29, No. 1, pp. 138-148, Mar. 2014.

[34] K. N. Gyftakis and J. C. Kappatou, "The zero-sequence current spectrum as an on-line static eccentricity diagnostic mean in Δ-connected PSH-induction motors," 9th IEEE SDEMPED, pp. 302-308, Valencia. Spain, 2013.

[35] K. N. Gyftakis and J. C. Kappatou, "A Novel and Effective Method of Static Eccentricity Diagnosis in Three-Phase PSH Induction Motors," *IEEE Trans. Ener. Conv*., Vol. 28, No. 2, pp. 405-412, Jun. 2013.

[36] I. K. Pallis, K. N. Gyftakis and J. C. Kappatou, "FEM study of the bar number impact on the stator core losses of the cage induction motor", 39th IECON, Vienna, Austria, pp. 2863-2868, Nov. 2013.